Development of an integrated analytical platform ~~of~~for clay ~~minerals~~mineral separation, characterization and ~~^{40}K/^{40}Ar~~K-Ar dating

Marie Gerardin[1], Gaetan Milesi[1], Julien Mercadier[1], Michel Cathelineau[1], Danièle Bartier[1]

[1]Université de Lorraine, CNRS, GeoRessources, 54520 Nancy, France

Correspondence to: Marie Gerardin (marie.gerardin@univ-lorraine.fr)

Abstract. Isotopic dating is a valuable method to constrain the timing of lithospheric processes: geodynamic episodes, ore deposition and geothermal regimes. The K-Ar dating technique has the main advantage of being applied to ubiquitous K-bearing minerals that crystallize in various temperatures, from magmatic to low temperatures. Clays are of significant interest among all K-bearing minerals, as they crystallize during various hydro-thermo-dynamic processes. Nonetheless, the dating of illites by the K-Ar method is not straightforward. K-Ar dates on illite usually rely on a mixed isotopic signal referring to various illitic populations that might have experienced isotopic resetting or re-crystallization processes. Therefore, reliable K-Ar dates on illite depend on (1) the grain size separation of large amounts of clay fractions, (2) the study of the morphology, mineralogy and crystallography, (3) the determination of precise K-Ar dates on each clay size fraction and (4) the meaningful interpretation of ages using either end-member ages or the Illite-Age-Analysis (IAA) method. This paper describes the instrumentation and methods recently developed at the GeoRessources laboratory of the University of Lorraine to obtain valuable ages on illite mixtures.

1 Introduction

The K-Ar dating method is based on the principle of the natural radioactive decay of the parent element ^{40}K to the daughter element ^{40}Ar. Potassium is an abundant element in the lithosphere. Its half-life of 1.248 ± 0.004 Ga (Grau Malonda and Grau Carles, 2002; Steiger and Jäger, 1977) is optimal for dating events over a wide range of geological times, from the early Precambrian to the Holocene (Dalrymple and Lanphere, 1969; Renne, 2000). Its abundance allows for detectable radiogenic argon accumulated after only several thousands of years. Argon is a noble gas, thus weakly bound to the mineral structure, but is retained in minerals because of its large atomic size (McDougall and Harrison, 1988, 1999). After sample melting, argon is measured by mass spectrometry (greatly developed after Nier's pioneering work in the 50's (Aldrich and Nier, 1948; Nier, 1940, 1950)). The application to many rock-forming minerals, the large range of geological times explored, and the reliability of the quantitative determination of K and ^{40}Ar make the K-Ar a popular dating technique developed worldwide. The early development of the K-Ar dating technique is extensively detailed ~~in~~by Schaeffer and Zähringer (1966) ~~or in~~and by Dalrymple and Lanphere (1969). More recently, Guillou et al. (2021) provided an extensive review of the protocol and method along with

its $^{40}Ar/^{39}Ar$ derived version (fully described by McDougall and Harrison (1988)). Although the fundamentals of the method are not reiterated here, some key considerations are highlighted for a clear understanding of this work.

The method relies on several ~~basic~~ assumptions. It is considered that (1) the decay of the parent nuclide, ^{40}K, is not affected by temperature or pressure changes, (2) the $^{40}K/K$ ratio (0.01167%) is constant over geological times, (3) the total amount of radiogenic ^{40}Ar measured in the mineral is produced by the decay of ^{40}K, (4) the isotopic ratios of atmospheric argon remained unchanged over geological times (Renne et al., 2009) and (5) the mineral or rock evolved as a closed system that did not loss or gain potassium or radiogenic argon (other than by radioactive decay). The latter might be ~~hypothetical~~false if the system has a complex geological and thermal history, but the resulting age can still provide valuable information on the thermal history, especially by using the Ar-Ar step-heating technique (McDougall and Harrison, 1988) (more details about the comparison of K-Ar and Ar-Ar ages on illite can be found in Clauer et al. (2012)). Given these assumptions, the age calculated indicates the length of time the daughter element has remained trapped in the mineral. This age ~~is then related~~relates to ~~a~~the crystallization event ~~(~~in the case of fast cooling ~~below~~(e.g., unaltered volcanic rocks), the closure ~~temperature~~time for slow cooling rocks (e.g., plutonic, metamorphic) or recrystallization during more recent geological hydrothermal or thermal episodes.

The main advantage of the K-Ar method is its application on K-rich minerals like phyllosilicates or feldspars, which crystallize in a wide range of temperatures from low (100-300°C) to magmatic temperatures. Clay-type phyllosilicates are of particular interest considering their ubiquity at the scale of the Earth system (Fig. 1). Since their chemistry depends on physical conditions (pressure and temperature) and on the type of host rocks, clay minerals are helpful markers of low-temperature geological processes such as basin diagenesis (Meunier et al., 2004; Perry, 1974), low-temperature metamorphism (Akker et al., 2021; Reuter and Dallmeyer, 1989), brittle fault deformation (Kralik et al., 1987; Monié et al., 2023) or hydrothermalism (Brockamp and Clauer, 2013; Zwingmann et al., 1998). The study of clay minerals, including their geochronology, is a powerful tool to constrain physical and chemical processes occurring at the micro- and nanoscale, improving our understanding of the evolution of the Earth system (Fig. 1).

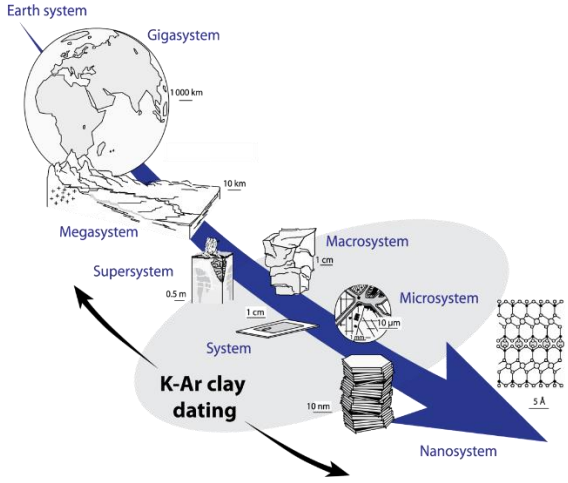

Fig. 1 – Potential of the K-Ar clay dating for the understanding of geological processes at different scale modified after (Velde and Meunier, 2008)

One of the main concern about clay minerals dating is the interpretation of their ages, since the data result often from a mixture of different clay populations (broadly mentioned in Clauer's work, (Clauer, 2020a, b) for the latest), which could be affected by partial isotopic and chemical resetting or by a recurrent crystallization history. As clearly explained in Clauer (2020a) and Hueck et al. (2022) latest reviews, K-Ar dating should only be performed on illite fractions properly separated by grain size. Mineralogical, morphological, crystallographic and geochemical information are also required prior to dating to interpret the ages. Those conditions substantiate the need to develop an integrated method coupling efficient clay separations and characterization with K-Ar dating.

This paper presents the platform developed at the GeoRessources laboratory (University of Lorraine) to date clay minerals using the K-Ar method. It includes (1) a detailed description of the argon ~~desorption~~extraction line and its technical characteristics along with the methodology to quantify radiogenic argon and (2) the specificity of the separation protocol and the characterization steps necessary to obtain valuable ages on illites. Finally, the method to extrapolate ages from illite mixed populations is presented and discussed in the light of literature data.

2 Description of the Argon ~~desorption~~extraction line and Methodology

2.1 Age calculation

The K-Ar age calculation is based on two separately determined analytical values, the content of potassium (^{40}K, radioactive parent) and of radiogenic argon (^{40}Ar*, ~~radioactive~~radiogenic daughter). Both analyses are destructive, therefore, two separate aliquots from the same sample are used. The homogeneity of these aliquots is granted by (1) preparing the two aliquots on the same day (same temperature and humidity conditions) and (2) using a large mass of aliquots to neglect the mineral heterogeneities. Classically, 100 mg is required for $\%K_2O$ determination by absorption spectroscopy, regardless of the age or potassium content. For argon measurements, the mass minimum depends on the ~~age and the~~ argon content~~.~~ (i.e., potassium concentration and age). A minimum of 1 to 3 mg is required for the clay fractions (<2µm) and 20 mg for materials with larger particle sizes (see 0 for details about mass accepted in the ~~desorption~~extraction line).

The equation to calculate the age is derived from the fundamental law of radioactive decay and is expressed as follows:

$$t\,[Ma] = \frac{1}{\lambda} ln\left(1 + \frac{\lambda}{\lambda_\epsilon + \lambda_\epsilon'} \frac{n_S^{40^*Ar}(t)[at/g]}{n_S^{40K}(t)[at/g]}\right) \times 10^{-6} \quad (1)$$

where t is the age expressed in million annus (Ma) (Nomade, 2017), $n_S^{40^*Ar}(t)$ is the number of atoms of ^{40}Ar* of argon per gram of sample at a time t, $n_S^{40K}(t)$ is the number of atoms of the radioactive ^{40}K per gram of sample at a time t and λ is the total decay constant of ^{40}K equal to $\lambda_\epsilon + \lambda_\epsilon' + \lambda_\beta$ (see Table 1 listing the values and descriptions of constants used for the age calculation). If not specified, all errors reported in this paper are expressed as one standard deviation.

Table 1 – Decay constants of ^{40}K and isotopic abundances of K and Ar.

Decay	Decay factor	Value	Reference
^{40}K to ^{40}Ca by β-	λ_β	4.96×10^{-10}	(Steiger and Jäger, 1977)
^{40}K to ^{40}Ar by electron capture	$\lambda_\epsilon + \lambda'_\epsilon$	5.81×10^{-11}	

Isotopic abundances	Description	Value	Reference
%(^{40}K/K)	Isotope 40 of potassium	0.01167%	(Garner et al., 1975)
%(^{40}Ar/Ar)	Isotope 40 of argon	99.60%	(Lee et al., 2006)

2.2 Measurement of the K_2O content

The potassium content is determined by optical emission spectrometry (ICP-OES) at the SARM (Service d'Analyse des Roches et des Minéraux) of the CRPG laboratory at Nancy, France. The reliability of their measurements is based on repeatable experiments on standard materials. The uncertainty on K_2O expressed in weight % in the 1-10% quantity range (typical of micas) is about 1.5% (2σ) for 100mg samples.

2.3 Description of the ~~desorption~~extraction line for argon quantification

Argon release is performed on an extraction-purification noble gas line. Preparation line specifications depend on each laboratory (Boulesteix et al., 2020; Cattani et al., 2019; Charbit et al., 1998a; Gillot and Cornette, 1986; Morgan et al., 2011; Phillips et al., 2017; Rouchon et al., 2008) but commonly comprise an induction furnace connected to a gas purification zone connected to a mass spectrometer. A schematic diagram of the ultra-high vacuum line developed at GeoRessources is shown in Fig. 2.

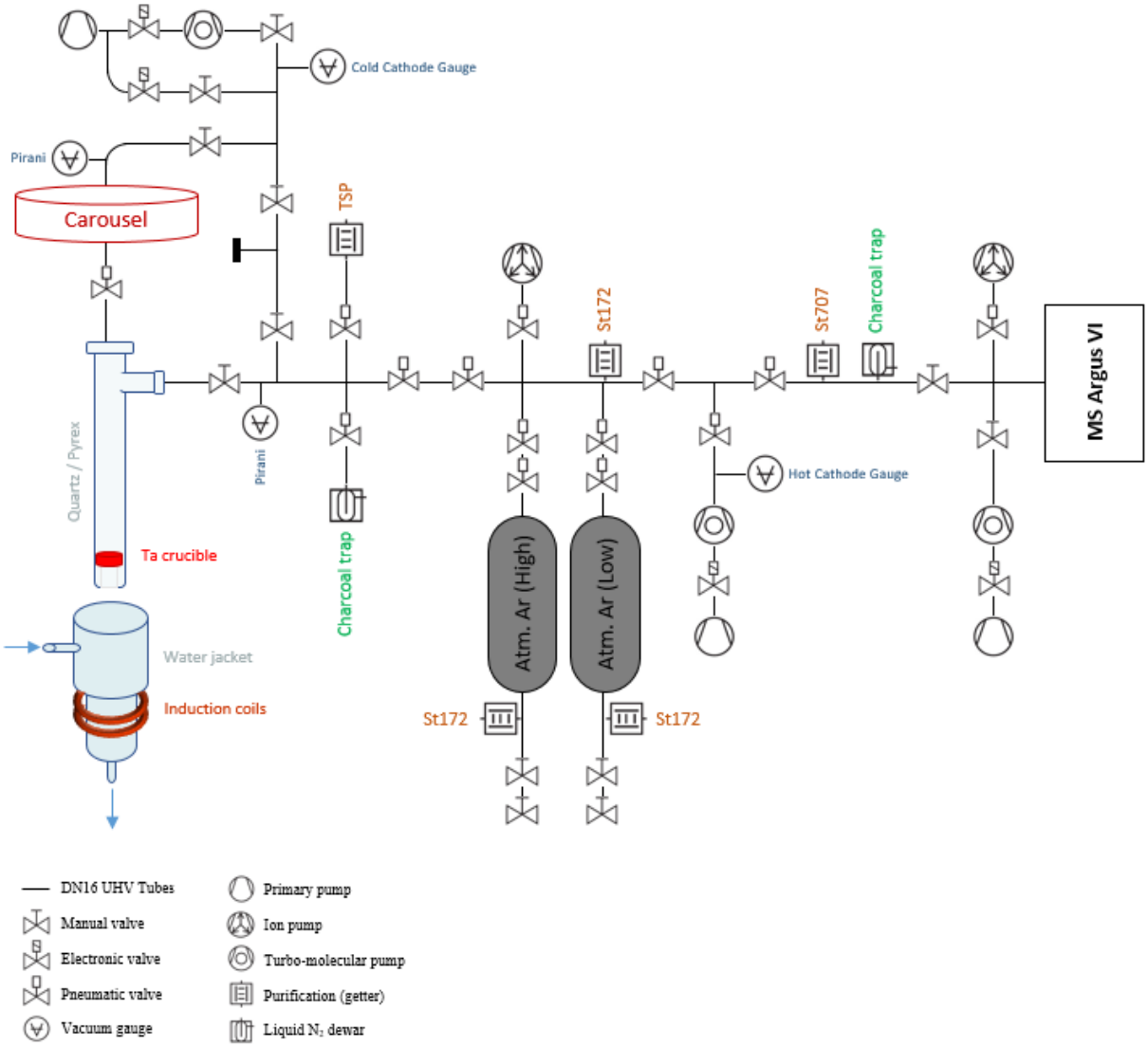

Fig. 2 – Schematic representation of the argon ~~desorption~~extraction line from the induction furnace to the mass spectrometer

Aliquots of samples are packed in a bending consisting of a 99.95% pure copper foil. They are placed under vacuum in individual pits of the carousel above the furnace. The samples are vacuum pumped using a turbo-molecular pump during 24h. This procedure was found to be equivalent to 24h backing at 105°C to remove adsorbed water from the sample (see 0).

Each of the ten pits connects to the furnace aperture by manual rotation of the carousel, dropping the sample by gravity into the Ta crucible. The carousel is isolated from the furnace by an UHV gate valve during heating.

The heating-melting setup is identical to the one originally settled in LSCE (Guillou et al., 2021) and in GEOPS (Gillot and Cornette, 1986) (Paris, France) for K-Ar dating. The samples are heated using a high-frequency furnace, the induction coil ringing a quartz tube containing a Ta crucible mounted on a Mo stool (to avoid direct contact with the quartz tube).

Gases other than argon that are released during ~~powder~~sample melting could be water vapor, hydrogen, oxygen, nitrogen, hydrocarbons, carbon dioxide and rare gases such as helium or krypton. The purification line next to the furnace is designed to trap all these gases in order to introduce only purified argon into the mass-spectrometer. The purification process is a two stage one, firstly extracted gases are exposed to a Ti sublimation pump and secondly to a GP50 SorbAC coupled to a St707 cartridge from SAES Getter operating at room temperature (see performance in Guillou et al., 2021). A charcoal trap cooled at -196°C (liquid nitrogen temperature) is used to transfer the gas from the furnace through the purification line. This cold trap is also useful for gases separation since H and He are not physio-sorbed on the charcoal surface. The efficiency of the purification is checked for each sample (see section 2.5).

After 45 minutes of gas clean-up, Ar isotopes 36, 38 and 40 are simultaneously analyzed using an ARGUS VI multi-collector mass spectrometer, that is a magnetic mass sector with a Nier-type source designed for operation in a static mode (Mark et al., 2009). The ARGUS VI spectrometer has 5 Faraday detectors and one CDD detector. Argon 40 is measured on the H2 Faraday cup fitted with a 10^{11} ohm resistor. Argon isotopes 36 and 38 are measured on the AX and the L2 cups respectively, both amplified with 10^{12} ohm resistors. All collectors are cross-calibrated by scanning the ^{40}Ar signal onto each cup. To compare one analysis to another, the analyzed volume has to be fixed and comprises the analyzing chamber of the mass spectrometer and the adjacent volume containing a Zr-Al getter and a charcoal trap. For argon analysis, the trap current is set at 170 µA with an electron potential of 60 eV. The acceleration potential is 4.5 kV.

2.4 Signal corrections

Figure 3 shows the signal measured on the H2 cup (^{40}Ar) of a dose of atmospheric argon entering the mass-spectrometer at t_0. The gas equilibrium state is achieved 8 seconds after t_0. An exponential regression is performed on the signal integrated over a period of 120 seconds to determine the signal at t_0.

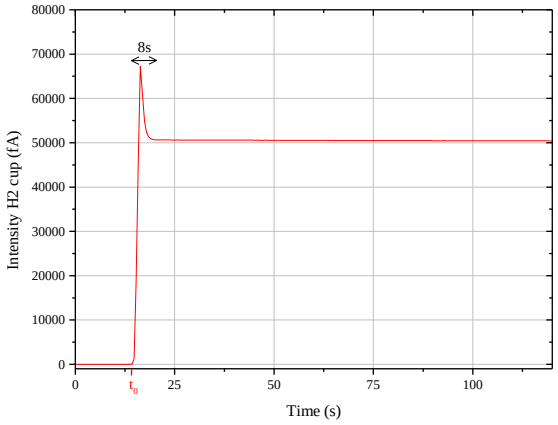

Fig. 3 – Intensity measured on the H2 cup (^{40}Ar) of 1DE (atmospheric argon) entering the mass-spectrometer

The sensitivity of the spectrometer depends on the ionization capacities of the source (Loveless and Russell 1969; Werner 1974; Holst et al., 1999; Rüedenauer 1972), on the gas pressure inside the analyzing chamber (Burnard and Farley, 2000) and on the detector type (Turrin et al., 2010). The intensity $I(^{x}Ar)$ has then to be corrected for the gas pressure effect.

The pressure dependence is assessed via the analysis of increasing number of calibrated air doses named "Dose-Equivalent" (DE) (Charbit et al., 1998). One DE is determined as the total amount of atmospheric argon contained in one aliquot expanded from an air container into the mass-spectrometer (see 0 for details about the air container). The intensity of the isotope 40 and the ratio 40/36 measured by the spectrometer from 1 to 5 accumulated DE (replicated) are shown in Fig. 4. Note that the depletion of the container for 5 doses is negligible considering isotopic measurement errors.

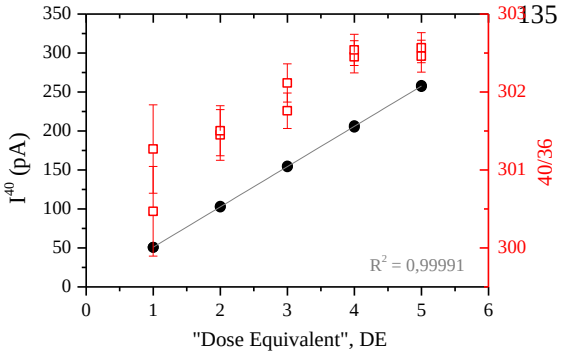

Fig. 4 – Signal of ^{40}Ar (black dots) and ^{40}Ar/^{36}Ar (red square) as a function of the number of accumulated DE sampled from the air container. The gray line is the linear fit applied to the experimental data. The maximum number of DE has been chosen considering the saturation value of the cups (400 pA for 40Ar cup and 40 pA for 38Ar and 36Ar) and the experimental handling capacities.

According to Fig. 4, the pressure dependence in the mass spectrometer is linear. The relation between the number of DE and the ^{40}Ar signal is given by the following equation:

$$I(^{40}Ar)(pA) = 51\text{~~663~~}.66 \times DE - \text{~~644~~}0.64 \quad (R^2 = 0.99991) \tag{2}$$

Note that this equation is valid when I(^{40}Ar) > 0.01 pA corresponding to the lowest signal measurable in the mass spectrometer (see the blank measurements at section 2.6 Blank measurements). The mass discrimination due to the ionization capacities of the electronic source does not significantly depend on the argon pressure. Considering uncertainties, the ratio 40/36 of atmospheric argon measured by the mass spectrometer (see Fig. 4) is considered to be constant at 302 ± 1.

2.5 Analysis procedure

The method applied here is based on the unspiked technique described by Cassignol and Gillot (1982). The argon measurement procedure is based on two independent analyses. The first is the measurement of the total ^{40}Ar released from the sample (Fig. 5 (a)). ~~The second~~The ratio R_S of the ^{40}Ar to ^{36}Ar and the DE_S (I_S^{40} corrected from the pressure effect) are calculated. The

second analysis is the measurement of a calibrated aliquot of atmospheric argon for the quantitative determination of the number of ^{40}Ar* atoms released from the sample (Fig. 5 (b)). During this step, the atmospheric ^{40}Ar/^{36}Ar ratio is measured by the mass spectrometer. This ratio is used directly to calculate the proportion of radiogenic argon $n_S^{40^*}$[%]. Also, the DE_p (I_p^{40} corrected from the pressure effect) is calculated.

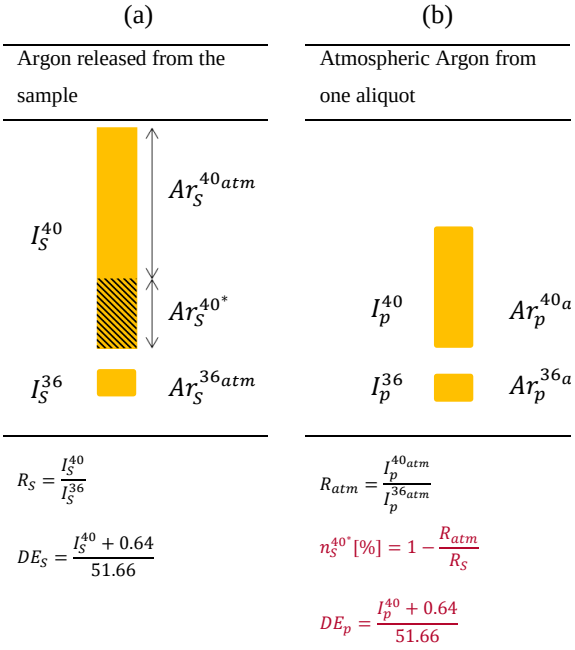

Fig. 5 – The two-step protocol for measuring radiogenic argon from rock samples (schematic representation derived from Gillot et al., 2006). *R* is the ratio of the m/z 40 to 36, $n_S^{40^*}$ ~~*[at]*~~[%] is the ~~number~~proportion of radiogenic argon ~~from~~in the sample and *DE* is the number of "Dose-Equivalent" deduced from the pressure calibration ~~and n_{DE} is the known amount of ^{40}Ar in one DE~~.

The number of ^{40}Ar* atoms released from sample per gram is then:

$$n_S^{40^*Ar}(t)[at/g] = n_S^{40^*}[\%] \times \frac{DE_S}{DE_P} \times n_{DE} \times \frac{1}{m} \quad (3)$$

Where m is the mass (g) and n_{DE} is the number of atoms of ^{40}Ar contained in one DE, which is calculated from the analysis of standard minerals. Here, this calculation relies on the analysis of 7 splits of *HD-B1* (Biotite from the Bergell granodiorite (Italy) (Fuhrmann et al., 1987; Schwarz and Trieloff 2007), split 26/7, grain size 200-500µm). We have recalculated the amount of ^{40}Ar* atoms per gram of *HD-B1* using the value of %K_2O determined by SARM following our protocol (K_2O = 9.52 ± 0.01 %, deviation of 0.6% from the published value, see Table 3) and the published age of t = 24.21 ± 0.32 Ma. n_{DE} was determined with an uncertainty of 0.5% achieved from the analysis of 7 *HD-B1* samples. This standard is periodically analyzed (1 over 10 unknown samples) to evaluate the deviation of n_{DE} relative to the time. Also, the pressure calibration is reiterated twice a year because of the depletion of the air container after the successive sampling of air aliquots.

The final check performed to validate an analysis is the verification of the efficiency of the gas cleanup. A mass scan over oxygen pics is performed for each sample using the ARGUS VI mass spectrometer. Validation is made if the oxygen peak m/e=16 is equal to or lower than that obtained when analyzing an aliquot of air.

2.6 Blank measurements

Blank measurements are periodically performed (1 over 10 samples) to verify that their argon composition is equivalent to the atmospheric one (i.e., the absence of radiogenic argon or any hydrocarbons or HCl remaining in the system). The protocol for blank measurement is exactly the same as for sample analyses. The results of the latest blank measurement are listed in Table 2. ^{40}Ar blank values are about 37 times less than those of 1 DE. The ^{40}Ar value of the unknowns are usually 10 times higher than the procedural blank. Table 2 also presents the electronic blank of the ARGUS VI mass spectrometer (signals on the H2, AX and L2 faraday detectors during pumping in the analyzing chamber). Because the composition of this blank is atmospheric, there is no need to deduce it from the signal of the sample. This induces that our measurement of the proportion of radiogenic argon ($n_S^{40^*}$[%]) is reduced. Our measurements so far lead to an underestimation from 1 to 10% of the proportion of the radiogenic argon initially contained in the sample. The underestimation of this value depends on the ^{40}Ar intensity ratio between the blank and the sample.

Table 2 – Intensity of line blanks compared to one DE

	I^{40} (fA)	I^{38} (fA)	I^{36} (fA)	40/36	40/38
Electronic Blank	7.3±0.4	-0.2±0.2	-1.0±0.2	-	-
Furnace Blank*	1 358.8±3.1	0.8±0.2	4.7±0.3	291±17	1 793±585
1 DE*	50 682±5	31.9±0.2	168.7±0.3	301.3±0.6	1 597±13

* signals corrected from the electronic blank

2.7 Reference materials

To our knowledge, no clay material is used as a reference material for K-Ar dating. Three phyllosilicates (muscovite and glauconite) of different ages were chosen instead to validate the protocol for measuring potassium and argon:

- *GL-O*, the glauconite of Odin from the Cauville cliff (France), reference material (Boulesteix et al., 2020; Odin, 1982);
- *BMus2*, a muscovite from the Bärhalde granite in the Black Forrest (Germany) (Rittmann, 1984), used as an in-house standard by (Schwarz and Trieloff, 2007);
- *PANXVII-3*: large muscovite selvage of quartz vein from Panasqueira (Portugal), in-house reference material dated by K-Ar (Snee et al., 1988) and more recently by Ar/Ar (Carocci et al., 2020).

Table 3 compares the ages obtained at GeoRessources to those from the literature of the three micas. The deviation from the literature of ages is less than 0.6%, which is lower than the uncertainty on the individual ages. These results validate the protocol used to measure potassium and radiogenic argon at GeoRessources.

Table 3 – Comparison of potassium content and ages of reference materials from the literature to those obtained at the SARM (CRPG) and GeoRessources

	%K2O Lit.	%K2O SARM	Age (Ma) Lit.	Age (Ma) GeoR
HD-B1 (Fuhrmann et al., 1987; Schwarz and Trieloff, 2007)	9.58 ± 0.02	9.52 ± 0.14	24.21 ± 0.32	-
B/Mus2 (Rittmann, 1984; Schwarz and Trieloff, 2007)	10.20	10.13 ± 0.15	328.5 ± 1.1	324.5 ± 3.2
GL-O (Odin, 1982)	6.56 ± 0.10	6.56 ± 0.10	95.0 ± 1.0	95.3 ± 1.0
PANXVII-3 (Carocci et al., 2020; Snee et al., 1988)	[9.91:10.67] ± 0.15	10.19 ± 0.15	296.3 ± 0.6	295.3± 1.5

3 Characterizing and Dating Illite

Clay fractions often contain a mixture of various ~~illites~~illite polytypes (Bailey, 1966), from possibly different origins (detrital and authigenic) and generations (Clauer, 2013). Common illite polytypes are 1Md, 1M and $2M_1$ (Reynolds and Thomson, 1993). In sedimentary units, the $2M_1$ illite polytype is considered as a detrital component due to its inert behavior in anchizonal to epizonal conditions (Bailey, 1966; Środoń and Eberl, 1984). It generally forms thicker platy crystallites shaped with irregular edges because they are subjected to some dissolution and erosional processes since crystallization (Clauer, 2013). The 1Md and 1M illite polytypes are considered as authigenic products formed under diagenetic to anchi-metamorphic conditions (Grathoff and Moore, 1996). They generally are platy to fibrous or lath-shaped (Peltz et al., 2022).

The separation of illite polytypes of different origin and generations is commonly attempted by separating illites by their particle size. XRD analyses and SEM observations are then performed on each size fraction with the main objective of relating mineralogical, crystallographic and morphological characteristics of the various illite populations to their crystallization ages.

3.1 Separation

A large amount of clay material is needed to perform XRD and K-Ar dating (see section 2.1). The following procedure is adapted from conventional separation techniques, enabling the production of large amounts of datable clays.

The sample material is first gently crushed using a mortar or different grinding machines depending on the stiffness of the sample. The so-crushed sample is added to deionized water for disaggregation in an ultrasonic bath for approximately 30 min. First, the coarse fractions (typically <2µm, 2-5 µm and 5-10 µm) are separated using gravity sedimentation based on the Stokes' law. For this, the disaggregated sample is poured into 2L cylinders placed in a thermo-statically controlled water tank. The GeoRessources laboratory owns two in-house designed water tanks that can carry six 2L cylinders each. Both are fitted with a tube system that connects the cylinders to a water pump, so to minimize the vibrations during sampling. To increase the efficiency of the separations and the yield of the suspensions (especially <2 µm), sampling of the same size fraction is performed several times on (1) the remaining solution and (2) the sampled solution. The <2 µm fraction is used to separate smaller fractions down to at least <0.1 µm, using the centrifuge Beckman-Coultier Avanti J-26S XP fitted with the JCF-Z

continuous flow rotor coupled to a calibrated peristaltic pump. This system allows for separating fractions directly during centrifugation. The time required for the procedure depends only on the volume of the solution to be separated. For example, the separation of 4L of solution generally lasts around 20 minutes, that is much faster than the several days needed with a classical separation technique (Poppe et al., 2001).

Fractions of 1-2 µm, 0.5-1 µm and < 0.5 µm were separated using the following parameters derived from (Viola et al., 2018): (3000 RPM; 350mL/min) for the < 1 µm, (1270 RPM; 250mL/min) for the < 0.5 µm, (6000 RPM; 230mL/min) for the < 0.2 µm and (10 000 RPM; 160mL/min) for the < 0.1 µm. Supernatants were then collected by centrifugation using the same centrifuge fitted with the JA-10 rotor with the following parameters: (6000 RPM; 10 min) for 1-2 µm, (7000 RPM; 10 min) for 0.5-1 µm and (9000 RPM; 20 min) for all fractions below 0.5 µm. The remaining excess of water is removed by air drying for a few days.

The efficiency of this separation protocol was monitored using a laser particle sizer and SEM observations. An example of the particle size proportion estimated in each separated fraction is shown in 0. As expected, a clear reduction of particle size is observed in the finer fraction.

Coupling the large capacities of the Stokes' benches to the centrifuge fitted with the continuous flow rotor increases our ability to collect large amounts of fractions, especially for the finest particles. For example, 200mg of the < 0.5 µm fraction was isolated from a 55g sample of fault gouge. Thus, this device and its associated separation protocol provide sufficient material for carrying out mineralogical characterization by XRD and K-Ar geochronology.

3.2 Structural and mineralogical characterization

SEM observations are performed on a TESCAN VEGA III equipped with an energy dispersive spectrometer (EDS) at the SCMEM (Service Commun de Microscopies Electroniques et de Microanalyses) at GeoRessources. First, thin sections, chips or polished sections of the whole rock are observed to obtain some structural and textural information. Secondly, the separated fractions are observed to (1) verify the size of the particles and (2) identify the morphology in each fraction. In the example given in 0, particles of the coarse fractions are platy and hairy in the finer fractions. One can assume at this stage that the sample contains two different polytypes of illite, possibly formed during successive geological events.

The different clays minerals are characterized by XRD using ~~the~~a Bruker D2 phaser equipped with a copper tube (35 kV, 40 mA). First, oriented mounts of the <2µm fractions are prepared following the methods of Moore and Reynolds (1997) and scanned over a range of 2 to 40°2θ with a step size of 0.02° 2θ and a 1 second count time per step. The identification of clay minerals is performed by comparing the diffractograms obtained under air-dry (AD), ethylene-glycol solvation (EG) and heating at 490°C (H). The comparison between (1) the AD and EG XRD diffractograms allows for the identification of the illite/smectite mixed-layer and (2) the AD and H for kaolinite identification (Holtzapffel, 1986). The values of the illite crystallinity are expressed by the Kübler index (KI) (Kübler, 1966). Randomly oriented powder are also mounted using a Si-low background sample holder with a 0.5 mm sample cavity. The sample holder is filled by the side as recommended by Grathoff and Moore (1996). The orientation randomness is checked by the ratio of the (002)/(020) illite peaks, which should

be low for non-oriented samples. This preparation is scanned over a range of 16 to 38° 2θ with a step size of 0.01 °2θ and a 3-second count time per step.

The peaks corresponding to the polytypes of illite (i.e. 2M1, 1M and 1Md) are identified using the approach proposed by Grathoff and Moore (1996). The proportion of the 2M1 and 1M polytypes are determined by obtaining the ratio of the area (or the height) of each polytype peaks to the area of the peak at 2.58Å, which is common to all illite polytypes. If the sum of 2M1 and 1M is smaller than 100%, the difference could be attributed either to the presence of the 1Md polytype, or to a slight preferential orientation. The obtained percentages of polytypes are cross-checked by comparing the experimental XRD diagram with the XRD patterns modeled by the Wildfire© software. If kaolinite is present in the clay fraction, the randomly oriented powder mount is heated to 550°C to prevent kaolinite peak from interfering with the hkl peak at 2.56 Å, and is rescanned.

3.3 Dating interpretation

3.3.1 Method

Each separated fraction is dated by the K-Ar method using the procedure described in the 2.5 section. As each fraction contains a mixture of illite polytypes, individual ages have little geological meaning. As mentioned in Hueck et al., (2022), two strategies can be applied to decipher geochronological information from the set of K-Ar ages.

The first is the limit age interpretation, generally applied when polytype quantification is not available. The date obtained on the finest fraction that most likely contains authigenic material, represents the maximum age of the illite authigenesis. Conversely, the date obtained on the coarsest fraction, most likely containing inherited material, represents the minimum age of the oldest illitization (detrital illite in the case of sedimentary units).

The second approach is the Illite-Age-Analysis (IAA) developed by Pevear (1992), in which end-member ages are determined by extrapolating the set of individual dates. Assuming that the sample contains a mixture of two illite populations, the end-member dates reflect the ages of the oldest and youngest geological events. The proportion of the two populations of illite must be determined so to evaluate the dates at 0% and 100% of one population (100% and 0% of the other). The extrapolation of end-member dates is generally performed using an error-weighted linear regression based on the least-square method applied to the set of individual dates (Van der Pluijm et al., 2001). The 90% confidence intervals are also calculated to define the error on the extrapolated ages. To consider the non-linearity of the age equation, some authors prefer to fit the data expressed as $e^{\lambda t}$ - 1 (Van der Pluijm et al., 2001; Ylagan et al., 2000; Haines and Van der Pluijm, 2023; Song and Sim, 2021), since it is a linear function with the ratio of radiogenic argon to potassium.

3.3.2 Application

To validate the IAA method applied at GeoRessources, two sets of dates published in the literature were used: (1) the set of dates of synthetic mixtures of two pure illite fractions, 2M1 (Wards – 428.0 ± 9.0 Ma) and 1M (RM-30 – 24.8 ± 0.6 Ma)

prepared by Ylagan et al. (2002) and (2) the set of dates of metapelites from the Rhenish massif from the recent study of Hueck et al. (2022). The ages obtained by fitting either the set of nominal dates or the exponential terms are presented in Fig. 6 along with literature data (measured and extrapolated ages). R-square is also shown in the figure as well as the number of dates available for the fit.

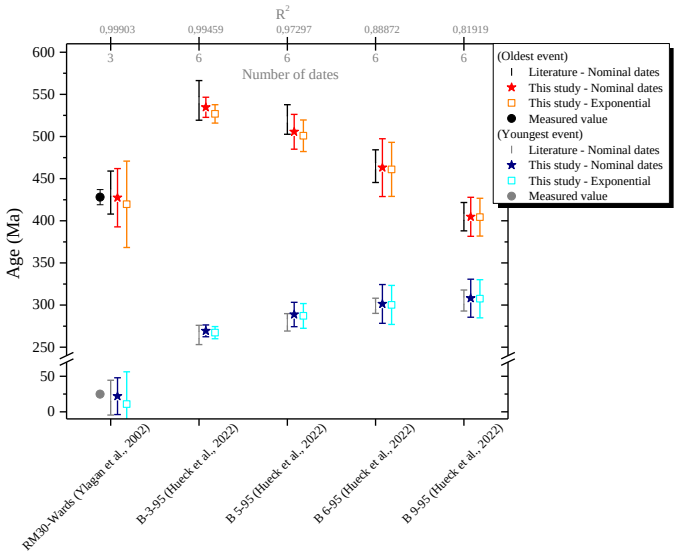

Fig. 6 – Comparison of extrapolated ages obtained by IAA between literature data and this study. The ages of RM-30 and Wards samples measured by Ylagan et al. (2002) are also shown.

Considering the uncertainties, one can reasonably state that the extrapolated ages calculated in this work are similar to those from the literature. Most notably, this present work successfully outputs the ages of the two pure illite fractions of Ylagan et al. (2002). Also, fitting the data using the exponential term does not significantly change the ages, as expected according to Ylagan et al. (2000).

In this work, fits are weighted by instrumental error ($w_i=1/\sigma^2$, σ being the individual date error). Consequently, the uncertainties will be reduced when fitting precise dates (sample B-3-95). Larger uncertainties than the published ones can be explained either by a limited set of dates, by high individual uncertainties on the dates (see samples B-6-95 and B-9-95, Hueck et al., 2022) or by the difference in the level of the confidence interval, 90% in this work and that of Ylagan and 68% for Hueck's study. Thus, to obtain valuable extrapolated ages, we recommend the following considerations:

- The fit should be weighted by the instrumental error;
- The level of confidence should be 90%;
- The data set should contain at least 4 dates (i.e. 4 separated fractions) and ideally, they will be distributed between 0 to 100% of one polytype.

Finally, it is essential to remember that the IAA method assumes that only two different polytypes are present in the illitic mixture. Also, the 2M1 illite must be either inherited or authigenic, and the 1M/1Md illite must be authigenetic (Hueck et al.,

2022). For the successful application of the IAA, those assumptions must be validated by complementary chemical, morphological and crystallographic data. More than two populations of illite might be detected either by the complementary analyses, or by the difficulty to obtain a proper linear regression on the set of dates obtained on the separated fractions (if each population relates to distinct geological events considering the precision of K-Ar dating).

4 Conclusion

Deciphering the origin of illites in a mixture of clays relies on (1) a proper separation of the clay material (at least 4 granulometric fractions) containing various proportions of illite material (ideally distributed between 0 to 100%), (2) a precise characterization of the mineralogy and the morphology by SEM, EDS and XRD of each size fraction, (3) the determination of a precise age of each size fraction by the K-Ar method and (4) the interpretation of the ages obtained by the IAA method enabling the identification of two geological events. Each of these four critical points was addressed in this paper in order to validate the method and protocols developed on the novel platforms of GeoRessources, which include the clay separation laboratory for large quantities and the K-Ar method.

This integrated method offers a powerful tool to provide constraints of various physical and chemical processes occurring at the micro- and nanoscale, improving our understanding of the evolution of the Earth system.

Appendix

A Mass ranges accepted in the ~~desorption~~extraction line depending on expected ages

Sample masses are measured on a Mettler XSU105DU with a resolution of 0.00001g in the 0-41 g range, which is calibrated every year by a certified company. The absolute error on the mass is set at 0.02mg.

The following plots illustrate the sample mass range accepted in the ~~desorption~~extraction line depending on age. Simulations are performed considering (1) the range of pressure accepted in the mass spectrometer and (2) the K_2O proportion of 10% (mica). For example, the mass of a large particle-sized sample with an expected age of about 500 Ma should range between 20 mg and 50 mg. For a sample of an expected age of about 1 Ma, the mass minimum should be 50 mg.

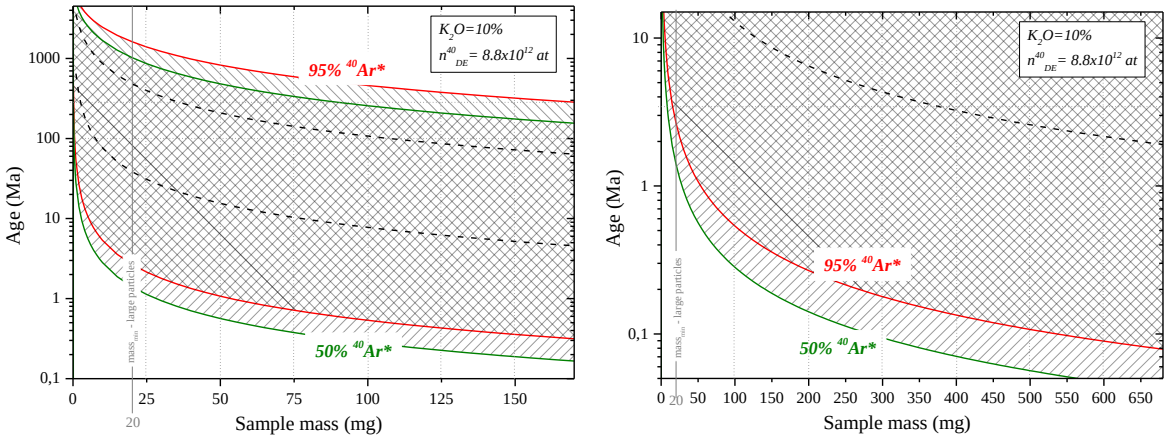

Fig. A1 – Ranges of mass accepted in the ~~desorption~~extraction line at GeoRessources depending on the expected age of the sample. Simulations are performed for 50 (green) and 95% (red) of radiogenic argon. The dense pattern represents the area of interest.

This wide range of masses and ages accepted in the ~~desorption~~extraction line is possible using three protocols implying additional gas expansion steps (when the argon pressure is high). The black dotted lines separate the areas of application of each protocol.

B Comparison of clay weight loss during annealing and vacuum pumping

This experiment was carried out on aliquots of < 2 µm clay particles. Aliquots (a to d) have been weighed before and after annealing at 105°C under air or vacuum pumping. Storage under vacuum or in the furnace lasts from 1 to 25 days. The loss of mass of the samples is presented in the Table 4. Independently of the mass of the aliquots, the furnace (A or B) and the storage duration, the weight losses after 105°C annealing and after vacuum pumping are close: around 0.76% under annealing and 0.92% under vacuum.

Table B1 – Comparison of clay weight loss during annealing and vacuum pumping

Sample Name	Mass	Treatment	Days	weight-loss (%)
WC448[<2]a	> 1g	Annealing at 105°C *Furnace A*	1	0.76
			2	0.75
			3	0.73
			7	0.65
			8	0.70
			13	0.82
WC448[<2]b	0.341 g	Annealing at 105°C *Furnace B*	1	0.76
WC448[<2]c	22.95 mg	Turbo-molecular pumping	1	0.92
			25	0.78
WC448[<2]d	51.01 mg		1	0.92
			25	0.96

A similar experiment was performed on GL-O (Odin's standard glauconite) (Odin, 1982). The weight loss after a few days of vacuum pumping lies between 2.51 and 3.14% (8 samples studied), in agreement with Zimmermann and Odin (1979) who

found a weight loss of about 3% by dehydration of the glauconite. The weight loss measured after vacuum storage of the samples is then due to the pumping of adsorbed gas and dehydration of samples.

Besides uncertainties, the slightly higher weight-loss values found on the clay aliquots stored under vacuum could be explained by the dehydration of clays that might be more efficient under vacuum than in a furnace at 105°C. Also, LOI (Loss Of Ignition) experiments performed at atmospheric pressure report the oxidation of Fe^{2+} that causes a slight weight increase, competing with weight loss by dehydration (Vandenberghe et al., 2010).

C Filling the calibrated air container

The calibration sector consists of a dried air container connected to an expansion valve. The amount of argon in the expansion valve after i individual dose taken from the container (n_i) is given by:

$$\begin{cases} n_i = n_0 \times \left(\dfrac{1}{1+\dfrac{v}{V_b}}\right)^i \\ n_0 = n_B \times \left(\dfrac{v}{V_b}\right) \end{cases} \quad (4)$$

Where n_0 is the amount of argon in the first dose, v is the volume of the expansion valve (approximated), V_b is the volume of the container and n_B is the initial amount of argon in the container (after filling).

Before filling the air container, the amount of argon expected in the expansion valve has been calculated so as to obtain a DE signal comparable to that of the samples. According to eq.(4), the amount of argon required in the expansion valve determines the amount of air to introduce in the container. Thus, the calibrated container has been specifically designed for the ARGUS VI mass spectrometer measurements tuned with specific source parameters.

The desired pressure of air in the container is calculated as follows:

$$P_b(air) \approx \frac{R \times T}{\%(Ar) \times \%(^{40}Ar) \times N_A} \times \left(\frac{1}{v}+\frac{1}{V_b}\right) \times \frac{I_{aliquot}(^{40}Ar)}{S} \quad (5)$$

Where $I_{aliquot}(^{40}Ar)$ (fA) is the intensity measured by the mass spectrometer of ^{40}Ar from the air aliquot, S (pA/at) is the sensitivity of the mass spectrometer, %(Ar) is the proportion of argon in air and %(^{40}Ar) is the proportion of the isotope 40 of argon.

To fill the container with this desired air pressure, a protocol of successive expansions and pumping was established using a set of two volumes V_o and V_x. Following this protocol, the air pressure in the container is:

$$P_b = P_0 \times \frac{1}{\left(\frac{V_0}{V_x}+1\right)^2} \times \frac{1}{\left(\frac{V_b}{V_x}+1\right)} \times \frac{1}{\left(\frac{V_0+V_x}{V_b}+1\right)^2} \quad (6)$$

$$P_b = 9.84 \pm 0.04\ Pa$$

Note that this pressure is too low to be measured by the manometers available at the laboratory. The two volumes V_0 and V_x were designed with the objective of minimizing the number of expansion and so, minimizing the error on the container pressure. Volumetric measurements yield values of 523.68±0.35 cc for V_0 and 47.20±0.03 cc for V_x. The volume of the container was determined by pressure measurement of nitrogen expanded from V_0+V_x to V_b (see Fig. C1 Fig. (a) for a scheme of the experimental setup). Successive measurements allow for a precise determination of V_b of 1947.1±3.8 cc. The scheme of the experimental setup for filling the air container is presented in C1(b). Note that the replacement of the valve V_0 by the SAES getter St172 does not significantly change the volume of the container (the volume difference is in the uncertainty).

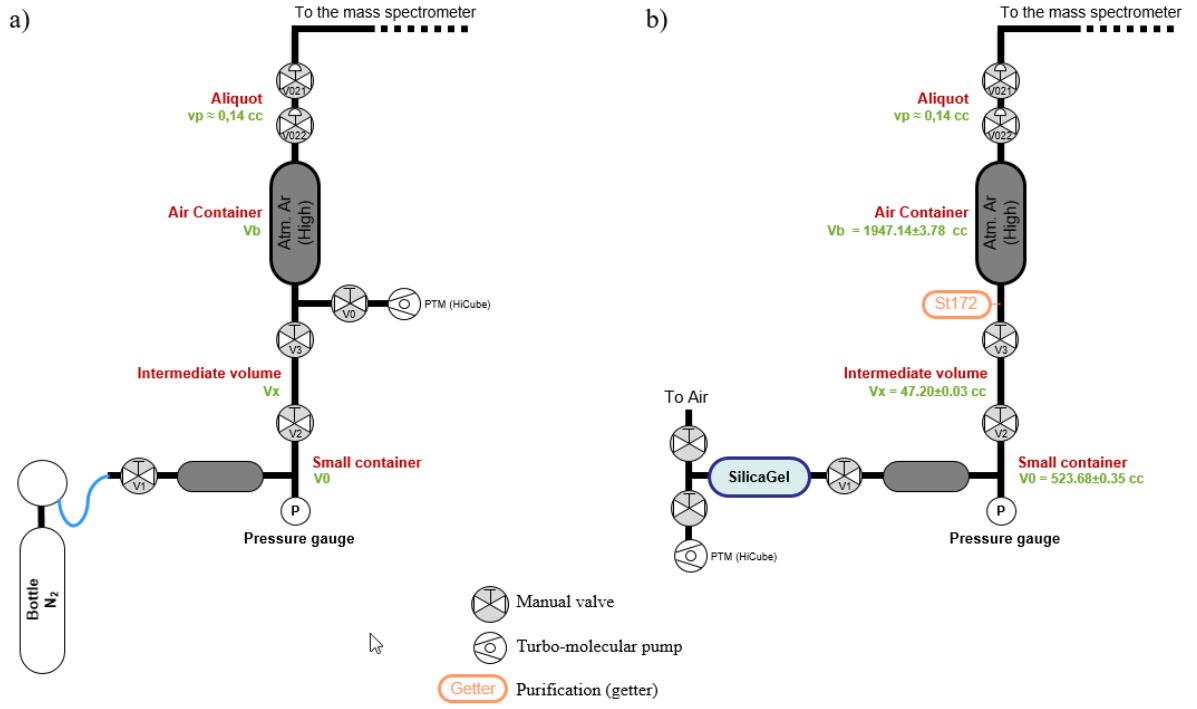

Fig. C1 – Schematic representation of the setup designed to a) measure the volume of the container and b) fill it with dried air.

D Laser diffraction analyses and SEM observations of the separated fractions

Granulometric analyses are performed at Chrono-Environnement (Besançon, France) on the LS230 Beckman Coulter laser particle size analyzer. An example of the particle size proportion estimated in each separated fraction is shown in Fig. D1. In the tested samples, only large clay particles were present, from 10 µm down to < 0.5 µm (an insignificant amount of clay were present in the < 0.2 µm fraction). The proportion of fine particles increases in the finer fractions to 75% of particles below 0.5 µm in the so-called < 0.5 µm fraction. However, in the so-called 2-5 µm fraction, 90% is above 2 µm with 50% above 5 µm.

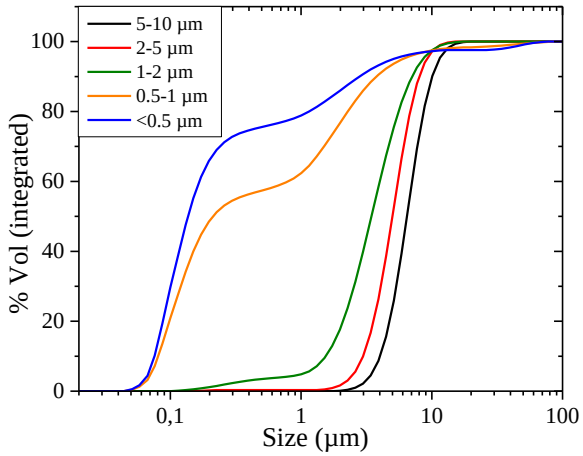

Fig. D1 –Particle size distribution in each separated fraction calculated by the Mie's theory on laser diffraction data.

The results of the laser diffraction are based on calculations using the Mie's theory hypothesis (Eremin, 2005), which considers spherical particles, isotropic and homogeneously distributed. Since clay minerals are platy to hairy shaped, the calculation of the particle size is naturally biased. Granulometric analysis based on laser diffraction is then not used for clay size measurements but rather for controlling the separation step.

SEM observations were performed on the whole rock of a fault gouge sample and on separated 5-10 µm, 2-5 µm and < 2 µm fractions. The separated fractions were observed after dropping the fractions diluted with ethanol on an SEM pad. Two morphologies can be identified on the whole rock: platy and hairy illites. The platy illite is dominant in the 5-10 µm and the hairy is dominant in the finer fraction. The 2-5 µm seems to contain the two morphologies, including platy illite with a smaller size than in the 5-10 µm fraction.

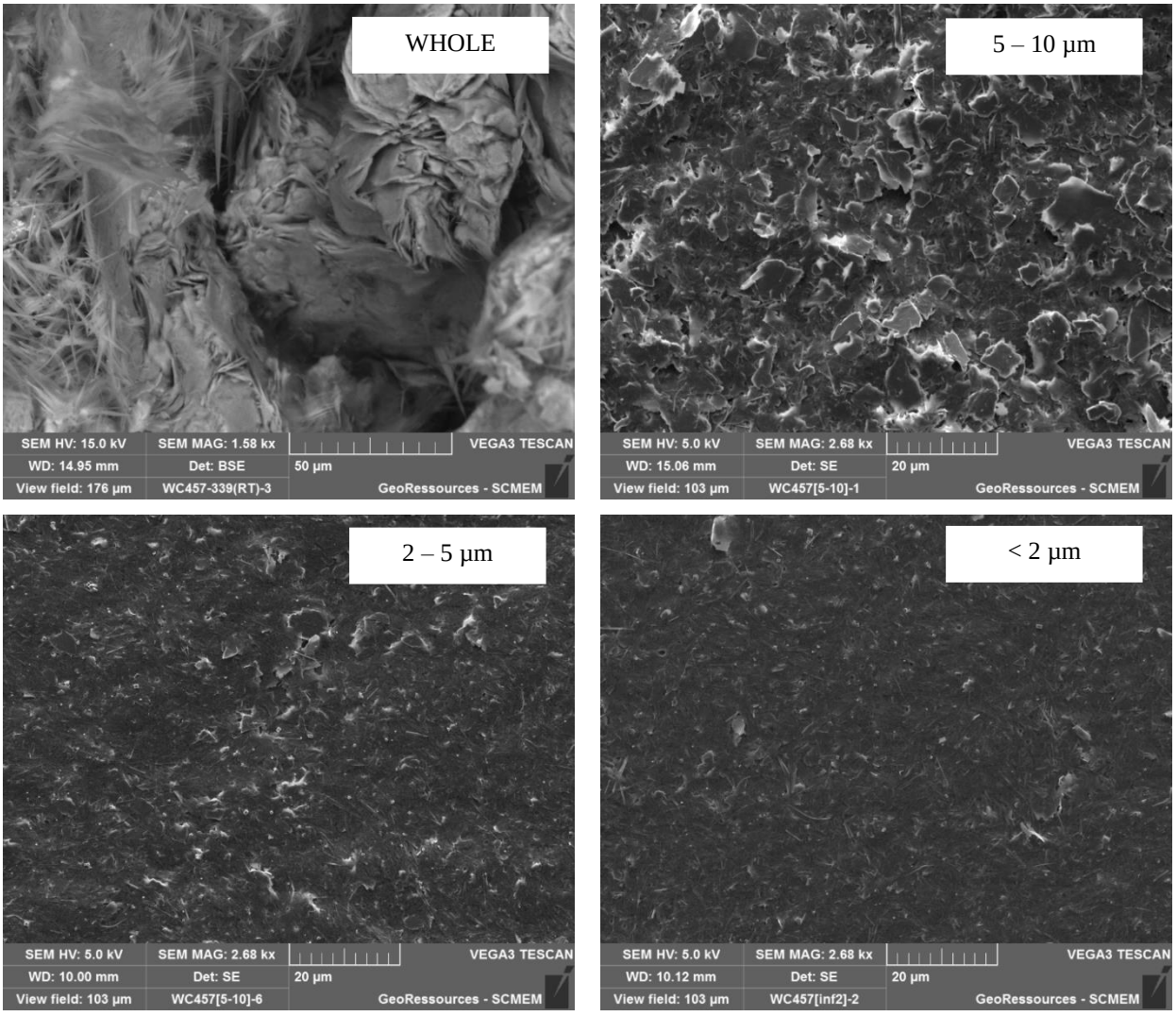

Fig. D2 – SEM observations of a fault gouge sample, whole rock and separated fractions 5-10µm, 2-5µm and 2µm. All fractions were observed at the same magnitude except the whole rock.

Competing interests

The authors declare that they have no conflict of interest.

Author contribution

Marie Gerardin: Project administration, Data curation, Formal analysis, Investigation, Methodology, Validation, Visualization, Writing – original draft preparation; **Gaétan Milesi**: Investigation, Methodology, Writing – original draft preparation; **Julien Mercadier**: Funding acquisition, Resources, Supervision; **Michel Cathelineau**: Funding acquisition,

Conceptualization, Resources, Supervision; **Danièle Bartier**: Formal analysis, Investigation, Methodology, Writing – original draft preparation.

Acknowledgment

The argon ~~desorption~~extraction setup was mainly funded by the LabEx RESSOURCES21 by the University of Lorraine and from Carnot and ERAMIN "MOSTMEG" funding programs. We want to acknowledge the important work of P. Robert (University of Lorraine) on his initial contribution on the development of the argon ~~desorption~~extraction line. We thank W. Schwarz (University of Heidelberg) for the discussions and the HD-B1 and B/Mus2 reference materials. We thank G. Viola (University of Bologna) and R. Van der Lelij (NGU, Norway) for discussing clay mineral separation, notably using the centrifuge. We thank Marguerite Perrey (Chrono-environnement, Besançon) for the laser diffraction analyses and the discussion about the size calculations. We thank N. Clauer (University of Strasbourg) for discussion about clay minerals dating by the K-Ar method and for reviewing this work. Many thanks to H. Guillou (LSCE, CEA Saclay) for the donation of his induction furnace and small Ti ceramic furnaces, and for all the discussion about K-Ar dating. Finally, a special thank is addressed to J-C. Lefèvre (GEOPS, Université Paris-Saclay) for the numerous discussions and meetings, and his significant technical help on the development of the argon ~~desorption~~extraction line.

References

Akker, I. V., Berger, A., Zwingmann, H., Todd, A., Schrank, C. E., Jones, M. W. M., Kewish, C. M., Schmid, T. C., and Herwegh, M.: Structural and chemical resetting processes in white mica and their effect on K-Ar data during low temperature metamorphism, Tectonophysics, 800, 228708, https://doi.org/10.1016/j.tecto.2020.228708, 2021.

Aldrich, L. T. and Nier, A. O.: Argon 40 in Potassium Minerals, Phys. Rev., 74, 876–877, https://doi.org/10.1103/PhysRev.74.876, 1948.

Bailey, S. W.: The Status of Clay Mineral Structures, Clays Clay Miner., 14, 1–23, https://doi.org/10.1346/CCMN.1966.0140101, 1966.

Boulesteix, T., Solé, J., Pi, T., and Cathelineau, M.: Reappraisal of the GL-O Reference Material for K-Ar Dating: New Insight from Microanalysis, Single-Grain and Milligram Ar Measurements, Geostand. Geoanalytical Res., n/a, https://doi.org/10.1111/ggr.12306, 2020.

Brockamp, O. and Clauer, N.: Hydrothermal and unexpected diagenetic alteration in Permian shales of the Lodève epigenetic U-deposit of southern France, traced by K–Ar illite and K-feldspar dating, Chem. Geol., 357, 18–28, https://doi.org/10.1016/j.chemgeo.2013.08.009, 2013.

Burnard, P. G. and Farley, K. A.: Calibration of pressure-dependent sensitivity and discrimination in Nier-type noble gas ion sources: TECHNICAL BRIEF, Geochem. Geophys. Geosystems, 1, n/a-n/a, https://doi.org/10.1029/2000GC000038, 2000.

Carocci, E., Marignac, C., Cathelineau, M., Truche, L., Poujol, M., Boiron, M.-C., and Pinto, F.: Incipient Wolframite Deposition at Panasqueira (Portugal): W Rutile and Tourmaline Compositions as Proxies for the Early Fluid Composition, Econ. Geol., https://doi.org/10.5382/econgeo.4783, 2020.

Cassignol, C. and Gillot, P.-Y.: Range and Effectiveness fo Unspiked Potassium-Argon Dating: Experimental Groundwork and Applications, John Wiley N. Y., 1982.

Cattani, F., Gillot, P.-Y., Quidelleur, X., Hildenbrand, A., Lefèvre, J.-C., Boukari, C., and Courtade, F.: In-situ K-Ar dating on Mars based on UV-Laser ablation coupled with a LIBS-QMS system: Development, calibration and application of the KArMars instrument, Chem. Geol., 506, 1–16, https://doi.org/10.1016/j.chemgeo.2018.12.010, 2019.

Charbit, S., Guillou, H., and Turpin, L.: Cross calibration of K–Ar standard minerals using an unspiked Ar measurement technique, Chem. Geol., 150, 147–159, 1998.

~~Charbit, S., Guillou, H., and Turpin, L.: Cross calibration of K–Ar standard minerals using an unspiked Ar measurement technique, Chem. Geol., 150, 147–159, 1998b.~~

Clauer, N.: The K-Ar and 40Ar/39Ar methods revisited for dating fine-grained K-bearing clay minerals, Chem. Geol., 354, 163–185, https://doi.org/10.1016/j.chemgeo.2013.05.030, 2013.

Clauer, N.: How Can Technical Aspects Help Improving K-Ar Isotopic Data of Illite-Rich Clay Materials into Meaningful Ages? The Case of the Dominique Peter Uranium Deposit (Saskatchewan, Canada), Geosciences, 10, 285, https://doi.org/10.3390/geosciences10080285, 2020a.

Clauer, N.: The post-Variscan tectonic-thermal activity in the southeastern metalliferous province of the French Massif Central revisited with K-Ar ages of illite, Ore Geol. Rev., 117, 103300, https://doi.org/10.1016/j.oregeorev.2019.103300, 2020b.

Clauer, N., Zwingmann, H., Liewig, N., and Wendling, R.: Comparative 40Ar/39Ar and K–Ar dating of illite-type clay minerals: A tentative explanation for age identities and differences, Earth-Sci. Rev., 115, 76–96, https://doi.org/10.1016/j.earscirev.2012.07.003, 2012.

Dalrymple, G. B. and Lanphere, M. A.: Potassium-argon dating: principles, techniques and applications to geochronology, Freeman, San Francisco., 1969.

Eremin, Y. A.: SCATTERING | Scattering Theory, in: Encyclopedia of Modern Optics, edited by: Guenther, R. D., Elsevier, Oxford, 326–330, https://doi.org/10.1016/B0-12-369395-0/00682-5, 2005.

Fuhrmann, U., Lippolt, H. J., and Hess, J. C.: Examination of some proposed K-Ar standards: 40Ar/39Ar analyses and conventional K-Ar data, Chem. Geol. Isot. Geosci. Sect., 66, 41–51, https://doi.org/10.1016/0168-9622(87)90027-3, 1987.

Garner, E. L., Murphy, T. J., Gramlich, J. W., Paulsen, P. J., and Barnes, I. L.: Absolute isotopic abundance ratios and the atomic weight of a reference sample of potassium, J. Res. Natl. Bur. Stand. Sect. Phys. Chem., 79A, 713, https://doi.org/10.6028/jres.079A.028, 1975.

Gillot and Cornette: The Cassignol technique for potassium—Argon dating, precision and accuracy: Examples from the Late Pleistocene to Recent volcanics from southern Italy, Chem. Geol. Isot. Geosci. Sect., 59, 205–222, 1986.

Gillot, P.-Y., Hildenbrand, A., Lefevre, J.-C., and Albore-Livadie C.: The K/Ar dating method : principle, analytical techniques, and application to Holocene volcanic eruptions in Southern Italy, Acta Vulcanol., 18, 55–66, 2006.

Grathoff, G. H. and Moore, D. M.: Illite Polytype Quantification using WILDFIRE© Calculated X-Ray Diffraction Patterns, Clays Clay Miner., 44, 835–842, https://doi.org/10.1346/CCMN.1996.0440615, 1996.

Grau Malonda, A. and Grau Carles, A.: Half-life determination of 40K by LSC, Appl. Radiat. Isot., 56, 153–156, https://doi.org/10.1016/S0969-8043(01)00181-6, 2002.

Guillou, H., Nomade, S., and Scao, V.: The 40K/40Ar and 40Ar/39Ar Methods, in: Paleoclimatology, edited by: Ramstein, G., Landais, A., Bouttes, N., Sepulchre, P., and Govin, A., Springer International Publishing, Cham, 73–87, https://doi.org/10.1007/978-3-030-24982-3_5, 2021.

Haines, S. H. and van der Pluijm, B. A.: Fault Gouge Dating in the Spanish Pyrenees: Fault Ages, Thrust Propagation Sequence, Wall-Rock Provenance, and Thermal Constraints, Tectonics, 42, e2022TC007251, https://doi.org/10.1029/2022TC007251, 2023.

Holst, B., Buckland, J. R., and Allison, W.: Spatial mapping in the electron-impact ion-source of a residual gas analyser, Vacuum, 53, 207–210, https://doi.org/10.1016/S0042-207X(98)00388-1, 1999.

Holtzapffel, T.: Minéraux argileux lattes : les smectites du domaine atlantique, Université d'Angers, 1986.

Hueck, M., Wemmer, K., Ksienzyk, A. K., Kuehn, R., and Vogel, N.: Potential, premises, and pitfalls of interpreting illite argon dates - A case study from the German Variscides, Earth-Sci. Rev., 232, 104133, https://doi.org/10.1016/j.earscirev.2022.104133, 2022.

Kralik, M., Klima, K., and Riedmüller, G.: Dating fault gouges, Nature, 327, 315–317, https://doi.org/10.1038/327315a0, 1987.

Kübler, B.: La cristallinite de l Illite et les zones tout a fait superieures du metamorphisme., Étages Tecton. Colloq. Neuchâtel 1966 Baconniere Neuchâtel, 105–121, 1966.

Lee, J.-Y., Marti, K., Severinghaus, J. P., Kawamura, K., Yoo, H.-S., Lee, J. B., and Kim, J. S.: A redetermination of the isotopic abundances of atmospheric Ar, Geochim. Cosmochim. Acta, 70, 4507–4512, https://doi.org/10.1016/j.gca.2006.06.1563, 2006.

Loveless, A. J. and Russell, R. D.: A strong-focussing lens for mass spectrometer ion sources, Int. J. Mass Spectrom. Ion Phys., 3, 257–266, https://doi.org/10.1016/0020-7381(69)85009-6, 1969.

Mark, D. F., Barfod, D., Stuart, F. M., and Imlach, J.: The ARGUS multicollector noble gas mass spectrometer: Performance for 40Ar/39Ar geochronology, Geochem. Geophys. Geosystems, 10, https://doi.org/10.1029/2009GC002643, 2009.

McDougall, I. and Harrison, T. M.: Geochronology and Thermochronology by the 40Ar/39Ar Method, Oxford University Press., 1988.

McDougall, I. and Harrison, T. M.: Geochronology and Thermochronology by the 40Ar/39Ar Method, Second Edition., Oxford University Press, Oxford, New York, 282 pp., 1999.

Meunier, A., Velde, B., and Zalba, P.: Illite K-Ar dating and crystal growth processes in diagenetic environments: a critical review, Terra Nova, 16, 296–304, https://doi.org/10.1111/j.1365-3121.2004.00563.x, 2004.

Monié, P., Münch, P., Milesi, G., Bonno, M., and Iemmolo, A.: 40 Ar/ 39 Ar geochronology of crustal deformation, Comptes Rendus Géoscience, 356, 1–29, https://doi.org/10.5802/crgeos.209, 2023.

Moore, D. M. and Reynolds, R. C.: X-Ray Diffraction and the Identification and Analysis of Clay Minerals, Oxf. Univ. Press, https://doi.org/10.1017/S0016756898501501, 1997.

Morgan, L. E., Postma, O., Kuiper, K. F., Mark, D. F., van der Plas, W., Davidson, S., Perkin, M., Villa, I. M., and Wijbrans, J. R.: A metrological approach to measuring 40Ar* concentrations in K-Ar and 40Ar/39Ar mineral standards: MEASURING 40Ar* CONCENTRATIONS, Geochem. Geophys. Geosystems, 12, n/a-n/a, https://doi.org/10.1029/2011GC003719, 2011.

Nier, A.: A Mass Spectrometer for Routine Isotope Abundance Measurements, Rev. Sci. Instrum., 11, 212–216, https://doi.org/doi:10.1063/1.1751688, 1940.

Nier, A.: A Redetermination of the Relative Abundances of the Isotopes of Carbon, Nitrogen, Oxygen, Argon, and Potassium, Phys. Rev., 77, 789–793, https://doi.org/10.1103/PhysRev.77.789, 1950.

Nomade, S.: Recommandation sur l'utilisation des unités de temps en sciences de la terre, Quaternaire, 28, 137–139, https://doi.org/10.4000/quaternaire.7972, 2017.

Odin, G. S.: Interlaboratory Standards for Dating Purposes, in: Numerical dating in stratigraphy, 123–148, 1982.

Peltz, M., Jacob, A., Grathoff, G. H., Enzmann, F., Kersten, M., and Warr, L. N.: A FIB-SEM Study of Illite Morphology in Aeolian Rotliegend Sandstones: Implications for Understanding the Petrophysical Properties of Reservoir Rocks, Clays Clay Miner., 70, 84–105, https://doi.org/10.1007/s42860-022-00174-9, 2022.

Perry, E. A.: Diagenesis and the K-Ar Dating of Shales and Clay Minerals, Geol. Soc. Am. Bull., 85, 827, https://doi.org/10.1130/0016-7606(1974)85<827:DATKDO>2.0.CO;2, 1974.

Pevear, D. R.: Illite age analysis, a new tool for basin thermal history analysis, International symposium on water-rock interaction, 1251–1254, 1992.

Phillips, D., Matchan, E. L., Honda, M., and Kuiper, K. F.: Astronomical calibration of 40Ar/39Ar reference minerals using high-precision, multi-collector (ARGUSVI) mass spectrometry, Geochim. Cosmochim. Acta, 196, 351–369, https://doi.org/10.1016/j.gca.2016.09.027, 2017.

van der Pluijm, B. A., Hall, C. M., Vrolijk, P. J., Pevear, D. R., and Covey, M. C.: The dating of shallow faults in the Earth's crust, Nature, 412, 172–175, https://doi.org/10.1038/35084053, 2001.

Poppe, L. J., Paskevich, V. F., Hathaway, J. C., and Blackwood, D. S.: A Laboratory Manual for X-Ray Powder Diffraction. Procedures - Separation of the silt and clay fractions by centrifugation, USGS, 2001.

Renne, P. R.: K-Ar and 40Ar/39Ar Dating, in: Quaternary Geochronology, American Geophysical Union (AGU), 77–100, https://doi.org/10.1029/RF004p0077, 2000.

Renne, P. R., Cassata, W. S., and Morgan, L. E.: The isotopic composition of atmospheric argon and 40Ar/39Ar geochronology: Time for a change?, Quat. Geochronol., 4, 288–298, https://doi.org/10.1016/j.quageo.2009.02.015, 2009.

Reuter, A. and Dallmeyer, R. D.: K-Ar and ^{40} Ar/ ^{39} Ar dating of cleavage formed during very low-grade metamorphism: a review, Geol. Soc. Lond. Spec. Publ., 43, 161–171, https://doi.org/10.1144/GSL.SP.1989.043.01.10, 1989.

Reynolds, R. C. and Thomson, C. H.: Illite from the Potsdam Sandstone of New York: A Probable Noncentrosymmetric Mica Structure, Clays Clay Miner., 41, 66–72, https://doi.org/10.1346/CCMN.1993.0410107, 1993.

Rittmann, K. L.: Argon in Hornblende, Biotit und Muskovit bei der geologischen Abkühlung – 40Ar/39Ar – Untersuchungen, Université de Heidelberg, 1984.

Rouchon, V., Lefèvre, J.-C., Quidelleur, X., Guérin, G., and Gillot, P.-Y.: Nonspiked 40Ar and 36Ar quantification using a quadrupole mass spectrometer: A potential for K–Ar geochronology, Int. J. Mass Spectrom., 270, 52–61, https://doi.org/10.1016/j.ijms.2007.11.009, 2008.

Rüedenauer, F. G.: Gas Scattering as a Limit to Partial-Pressure Sensitivity, J. Vac. Sci. Technol., 9, 215–215, https://doi.org/10.1116/1.1316557, 1972.

Schaeffer, O. A. and Zähringer, J.: Potassium argon dating, Springer-Verlag, 278 pp., 1966.

Schwarz, W. H. and Trieloff, M.: Intercalibration of 40Ar–39Ar age standards NL-25, HB3gr hornblende, GA1550, SB-3, HD-B1 biotite and BMus/2 muscovite, Chem. Geol., 242, 218–231, https://doi.org/10.1016/j.chemgeo.2007.03.016, 2007.

Snee, L. W., Sutter, J. F., and Kelly, W. C.: Thermochronology of economic mineral deposits; dating the stages of mineralization at Panasqueira, Portugal, by high-precision 40 / 39 Ar age spectrum techniques on muscovite, Econ. Geol., 83, 335–354, https://doi.org/10.2113/gsecongeo.83.2.335, 1988.

Song, Y. and Sim, H.: Illite-Age-Analysis (IAA) for the Dating of Shallow Faults: Prerequisites and Procedures for Improvement, Minerals, 11, 1162, https://doi.org/10.3390/min11111162, 2021.

Środoń, J. and Eberl, D. D.: Illite, in: 12. ILLITE, vol. 13, Micas. Rev. Mineral, 495–544, https://doi.org/10.1515/9781501508820-016, 1984.

Steiger, R. and Jäger, E.: Subcommission on geochronology: convention on the use of decay constants in geo-and cosmochronology, Earth Planet. Sci. Lett., 36, 359–362, 1977.

Turrin, B. D., Swisher, C. C., and Deino, A. L.: Mass discrimination monitoring and intercalibration of dual collectors in noble gas mass spectrometer systems, Geochem. Geophys. Geosystems, 11, https://doi.org/10.1029/2009GC003013, 2010.

Vandenberghe, R. E., de Resende, V. G., da Costa, G. M., and De Grave, E.: Study of loss-on-ignition anomalies found in ashes from combustion of iron-rich coal, Fuel, 89, 2405–2410, https://doi.org/10.1016/j.fuel.2010.01.022, 2010.

Velde, B. and Meunier, A.: The Origin of Clay Minerals in Soils and Weathered Rocks, Springer Berlin Heidelberg, Berlin, Heidelberg, https://doi.org/10.1007/978-3-540-75634-7, 2008.

Viola, G., Torgersen, E., Mazzarini, F., Musumeci, G., Lelij, R., Schönenberger, J., and Garofalo, P. S.: New Constraints on the Evolution of the Inner Northern Apennines by K-Ar Dating of Late Miocene-Early Pliocene Compression on the Island of Elba, Italy, Tectonics, 37, 3229–3243, https://doi.org/10.1029/2018TC005182, 2018.

Werner, H. W.: A study on mass discrimination in a magnetic sector mass spectrometer, Int. J. Mass Spectrom. Ion Phys., 14, 189–203, https://doi.org/10.1016/0020-7381(74)80007-0, 1974.

Ylagan, R. F., Pevear, D. R., and Vrolijk, P. J.: Discussion of “Extracting K-Ar ages from shales: a theoretical test,” Clay Miner., 35, 599–604, https://doi.org/10.1180/000985500546918, 2000.

Ylagan, R. F., Kim, C. S., Pevear, D. R., and Vrolijk, P. J.: Illite polytype quantification for accurate K-Ar age determination, Am. Mineral., 87, 1536–1545, https://doi.org/10.2138/am-2002-11-1203, 2002.

Zimmermann, J.-L. and Odin, G. S.: Cinétique de la libération de l'argon de l'eau et des composés carbonés dans le matériel de référence glauconite GL-O, Bull. Minéralogie, 102, 48–55, https://doi.org/10.3406/bulmi.1979.7250, 1979.

Zwingmann, H., Clauer, N., and Gaupp, R.: Timing of fluid flow in a sandstone reservoir of the north German Rotliegend (Permian) by K-Ar dating of related hydrothermal illite, Geol. Soc. Lond. Spec. Publ., 144, 91–106, 1998.